Scientific Contributions Oil & Gas, Vol. 49. No. 1, March: 475 - 491

SCIENTIFIC CONTRIBUTIONS OIL AND GAS

Testing Center for Oil and Gas
LEMIGAS

Journal Homepage:http://journal.lemigas.esdm.go.id
ISSN: 2089-3361, e-ISSN: 2541-0520

Application of Computational Fluid Dynamics Simulation in The Case of Upward Vertical Core Annular Flow of Oil-Water System

Cindy Dianita[1,2], Rana Nur Fatimah[1,2] and Abdul Wahid[1,2]

[1]Process Systems Engineering Laboratory, Faculty of Engineering, Universitas Kampus UI Baru, Department of Industrial Engineering, Faculty of Engineering, Depok, West Java 16424, Indonesia.

[2]Department of Chemical Engineering, Faculty of Engineering, Universitas Indonesia, Kampus UI Baru, Depok, 16424, Indonesia.

Corresponding author: Cindy Dianita (cindydianita@ui.ac.id)

Manuscript received: January 26th, 2026; Revised: February 20th, 2026
Approved: February 23th, 2026; Available online: March 18th, 2026; Published: March 18th, 2026.

ABSTRACT - The energy required to transport heavy oil through pipelines can be significantly lowered by applying the core-annular flow (CAF) technique, in which a layer of water surrounds the oil as it moves through the pipe. This research investigates the behavior of upward oil–water flow in vertical pipelines using three-dimensional computational fluid dynamics (CFD) simulations. The numerical analysis is conducted based on previously published experimental studies. Validation has been completed to ensure the visual and numerical consistency of the observed interfacial wave geometry. This CFD work captures the wavy bamboo CAF pattern, illustrating the effect of buoyancy and pressure gradient in upward vertical flow, as demonstrated by experimental results. The present CFD simulation results indicate a relatively stable velocity distribution, where the central region of the pipe contains the highest concentration of oil. In addition, the absolute pressure gradually decreases along the length of the pipe, while the wall shear stress remains relatively low. The influence of gravity affecting the flow is investigated, showing a higher pressure drop compared to gravity-free flow. Compared with single-phase heavy oil transport, the CAF technique demonstrates significantly higher efficiency, achieving energy savings exceeding 90%. Furthermore, the three-dimensional simulation developed in this study provides more detailed flow pattern representation and more reliable hydrodynamic predictions than those obtained from earlier two-dimensional analyses.

Keywords: CFD simulation, core-annular flow, oil-water, upward flow, vertical pipe

How to cite this article:

Cindy Dianita, Rana Nur Fatimah, and Abdul Wahid 2026, Application of Computational Fluid Dynamics Simulation in The Case of Upward Vertical Core Annular Flow of Oil-Water System, Scientific Contributions Oil and Gas, 49 (1) pp. 475-491. DOI doi.org/10.29017/scog.v49i1.1971.

INTRODUCTION

Heavy and extra-heavy crude oils have traditionally been less utilized due to their very high viscosity and complex chemical characteristics. These properties make their extraction, transportation, and refining processes more difficult and expensive (Widarsono et al., 2021; Susantoro et al., 2022). Pipeline transport is the most practical method, yet heavy crude suffers from low mobility and wax or bitumen deposition along pipe walls (Silva et al. 2020). Traditional methods, including dilution and thermal treatment, can lower the viscosity of heavy oils; however, these techniques typically involve significant operational expenses.

A more efficient alternative is to transport heavy oil together with a low-viscosity, immiscible fluid, such as water. Introducing water into the flow can greatly decrease the pressure gradient. The most effective arrangement is known as core–annular flow (CAF), in which a surrounding layer of water acts as a lubricant for the highly viscous oil flowing in the central core (Xie et al., 2023; Kim & Park, 2024). This mechanism reduces the pressure drop to levels similar to single-phase water flow. Core Annular Flow (CAF) has been used since 1904. One notable example is a commercial pipeline system in Indonesia that transports approximately 40,000 barrels of oil per day across a distance of 238 km. This technology is applied in several industries, including petroleum, petrochemicals, food processing, and pharmaceuticals, and palm-oil industries, offering notable energy and cost savings (Coelho et al. 2019).

In vertical pipelines, core annular flow (CAF) generally shows greater stability because buoyancy forces help support and accelerate the oil core. This differs from horizontal pipelines, where variations in density tend to shift the core away from the center, leading to eccentric flow. Rodriguez and Bannwart (2006) experimentally investigated interfacial waves under vertical CAF conditions, and subsequent CFD studies have reproduced these conditions for deeper analysis (Gupta, Turangan & Manica 2016).

Although two-dimensional CFD models can offer basic insights into the flow behavior, they are unable to fully represent the complex three-dimensional characteristics of core annular flow (CAF), such as stratification, mixing processes, and detailed wall shear stress distribution. 3D simulations provide a more realistic representation of the flow structure and hydrodynamics (Dianita et al. 2025). Therefore, this study applies three-dimensional CFD modeling using the experimental setup reported by Rodriguez and Bannwart (2006). The simulation results are used to obtain velocity distributions, pressure profiles, phase volume fractions, and shear stress data, which are subsequently analyzed to better understand the hydrodynamic behavior and energy characteristics of the system. Validation is conducted visually and numerically by referencing experimental data and established empirical correlations.

METHODOLOGY

In this study, CFD simulations are carried out using ANSYS Fluent. The simulation procedure in ANSYS Fluent generally consists of three primary stages: pre-processing, numerical solution (solver), and post-processing (ANSYS Inc., 2023a). CFD simulation with ANSYS Fluent involves pre-processing steps to prepare geometry and mesh, a solver to calculate fluid flow based on the selected physical model, and post-processing to analyse and visualise the results. The input parameters for the model setup and solution procedure are summarized in Table 1. The geometry and flow

condition in this simulation work are adapted from Rodriguez and Bannwart (Rodriguez & Bannwart 2006) while the parameter of the simulation is summarized in Table 1.

Computational domain

The pre-processing stage involves creating the model geometry and preparing the computational mesh that will be used for the analysis. The vertical pipe domain is adapted from the experimental setup of Rodriguez and Bannwart (2006), with a total length of 568 mm and a core radius of 11.36 mm. To obtain a higher-quality mesh, the annulus region is split into four separate sections, as illustrated in Figure 1. The geometry was developed using Design Modeler in ANSYS Fluent (Rodriguez and Bannwart, 2006).

Once the geometry is finalized, it is imported into the meshing stage. Square elements are applied in the core region, while the mesh is progressively refined in the radial direction toward the pipe wall. This refinement helps capture the wave contours more accurately, particularly within the annular region. A multizone meshing method is applied to produce a hexahedral-dominant grid. Hexahedral elements are selected because they are more effective at representing curved geometries and provide more consistent estimates of contact pressure and shear stress, independent of factors such as friction or material incompressibility (Lintermann 2021).

Model validation

A grid independence test was performed using four mesh sizes: 35,334; 58,964; 94,970; and 166,760 cells. When three or more mesh levels are applied, a refinement factor greater than 1.3 between the coarse and fine meshes is typically regarded as sufficient. The evaluated outputs

Table 1. Summary of input parameter.

Parameter		Input
Model	Solver	Multiphase (Primary: water; Secondary: oil) Volume of Fluid (VOF) Volume Fraction Parameters: Explicit; Courant Number = 0.25 Surface Tension Coefficient = 0.02 N/m; Continuum Surface Force; Wall Adhesion
	Viscous	Laminar
Material	Water	$\rho = 998.2$ kg/m^3 $\mu = 0.001$ kg/ms
	Oil	$\rho = 930$ kg/m^3 $\mu = 0.5$ kg/ms
Operating Conditions	Operating Pressure	1.01325×10^5 Pa
Boundary Conditions	Water Inlet	Velocity magnitude = 0.2146 m/s
	Oil Inlet	Velocity magnitude = 0.3220 m/s
	Outlet	1.01325×10^5 Pa
	Wall	Stationary, No slip condition
Control	Solution	Pressure-velocity coupling (PISO) Discretization Gradient least square cell based Pressure PRESTO! Momentum second order upwind Volume fraction geo-reconstruct Transient formulation first order implicit
	Initialize	Standard initialization Oil volume fraction = 0
		Absolute criteria
Parameter		**Input**
Control	Residual	x-velocity = 10^{-3} y-velocity = 10^{-3} z-velocity = 10^{-3} Continuity = 10^{-3}

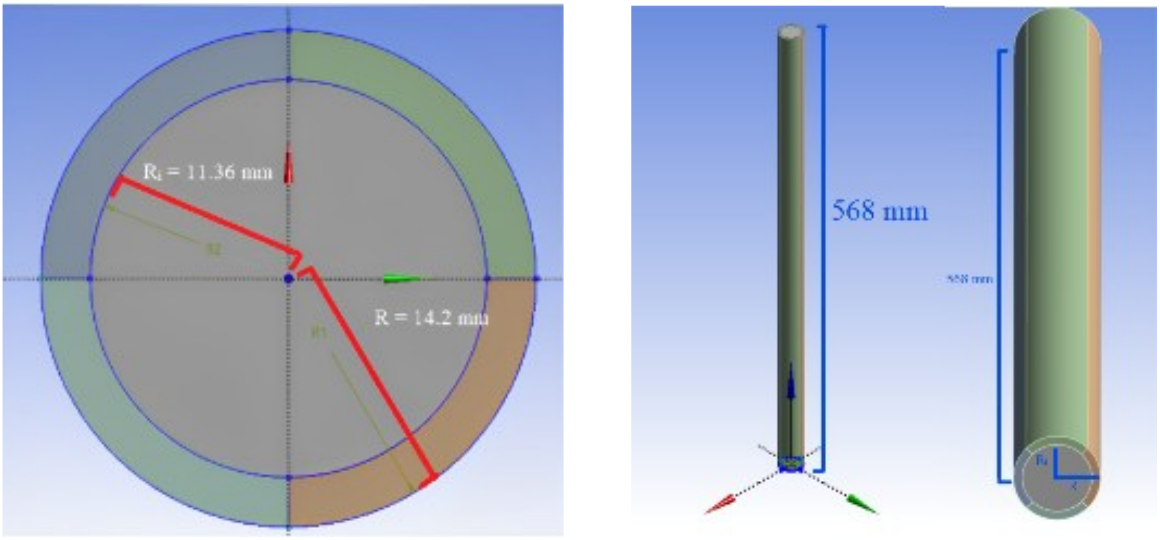

(a) (b)

Figure 1. Cross-section of pipe and isometric view of geometry.

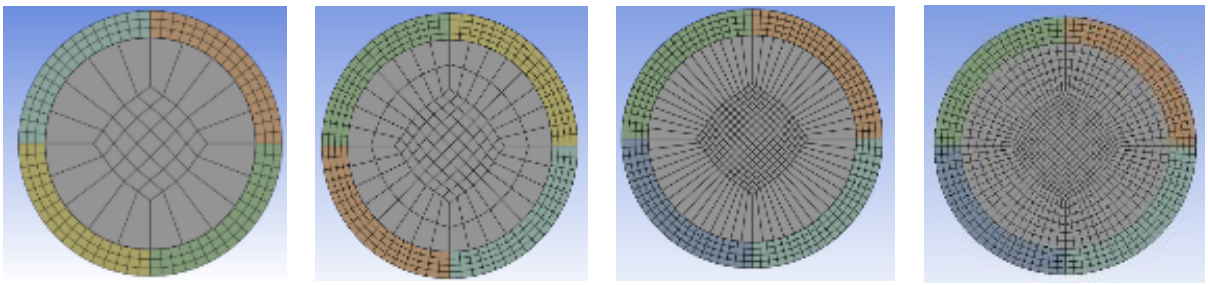

(a) (b) (c) (d)

Figure 2. Face detail of meshes with (a) 35,334; (b) 58,964; (c) 94,970; (d) 166,760 numbers of elements.

include maximum velocity, average velocity, and pressure gradient. Figures 2 and 3 illustrate the bottom view and axial view of the mesh for several different element quantities.

Figures 4 and 5 compare the velocity and pressure data obtained from the four mesh sizes. The mesh containing 94,970 cells exhibits only minimal differences when compared with the finest mesh of 166,760 cells. Consequently, this mesh configuration is chosen for all subsequent simulations. The quality of the mesh was evaluated based on three parameters: skewness, aspect ratio, and orthogonal quality.

Lower skewness values indicate a shape closer to the ideal, while orthogonal quality ranges from near 0 for the poorest cells to 1 for the best (ANSYS Inc. 2021; ANSYS Inc. 2023b). The aspect ratio indicates the degree to which a cell is stretched, and for stable numerical calculations it should be kept below 35:1. As presented in Table 2, the evaluated mesh satisfies the recommended standards, as the values of skewness, orthogonal quality, and aspect ratio all fall within acceptable limits.

Table 2. Metric values of the mesh quality.

Metric	Value		
	Minimum	Average	Maximum
Skewness	5.6547E-9	6.167E-2	4.6024E-1
Orthogonal Quality	6.8860E-1	1	9.7254×10^{-1}
Aspect Ratio	1.3973	5.965	7.202

Prior to examining the simulation results, the entrance length and the transient (time-dependent) behavior are evaluated first. The entrance length represents the region in which the flow adjusts from its initial state to a fully developed velocity profile, and its value depends on parameters such as Reynolds number, pipe geometry, and flow conditions (Çengel & Ghajar 2025).

Using the oil's density, viscosity, and superficial velocity, the Reynolds number was determined to be 11.0930. This value is significantly lower than the critical limit of 2300, which indicates that the flow regime is laminar. For laminar conditions, the nondimensional hydrodynamic entrance length (Le) can be determined using Eq. 1 as referenced in Çengel and Ghajar (2025).

$$L_e = 0.0575 \times Re \times D \quad (1)$$

Therefore,

$$L_e = 0.01811\ m = 18.11\ mm$$

In this context, Re represents the Reynolds number, D denotes the diameter of the pipe, and Le refers to the entrance length. Hence, the flow profile is fully developed at pipe lengths of more than 18.11 mm. The data used in this study were obtained from a 550 mm section of the pipe located near the outlet. A time-dependent test in CFD refers to the analysis of fluid flow and its associated variables as they change over time, typically using simulations or experimental methods. In this case, velocity profile data is taken at a length of 550 mm. Speed does not experience significant fluctuations after 4.5 seconds. The analysis time was then set to 5 seconds.

Solver model

In this study, the Volume of Fluid (VOF) approach was integrated with the Continuum Surface Force (CSF) model to represent and analyze the behavior of the interface formed between two immiscible fluids. The VOF formulation was implemented assuming no interphase mass transfer

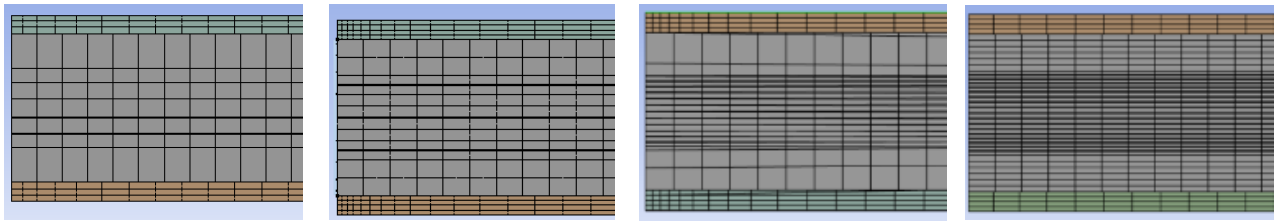

(a) (b) (c) (d)

Figure 3. Cross-sectional mesh detail in axial direction with (a) 35,334; (b) 58,964; (c) 94,970; (d) 166,760 numbers of elements.

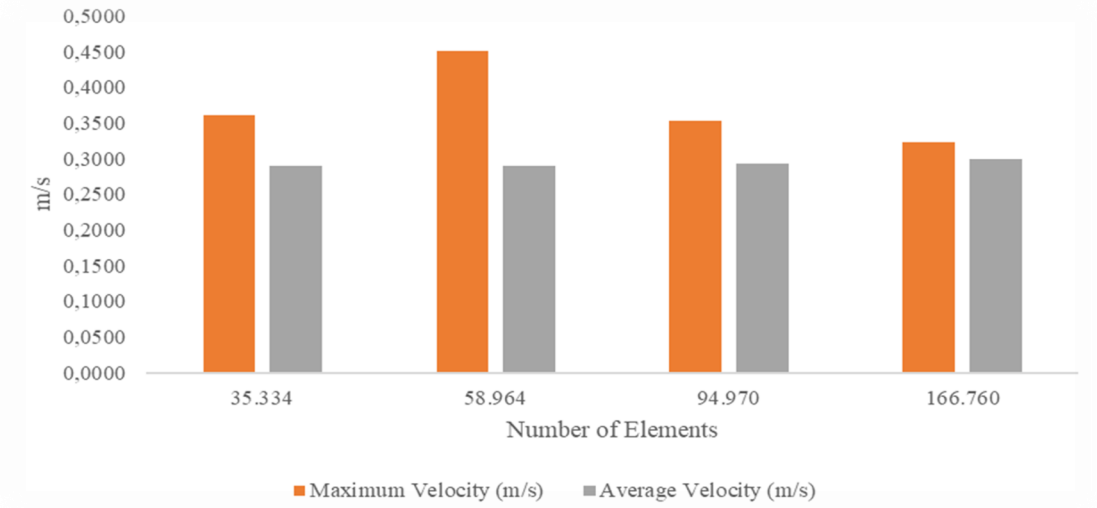

Figure 4. Comparison of the velocity data of various numbers of element.

between the fluids. The governing equations include the continuity equation (Eq. 2) and the momentum equation (Eq. 3).

$$\frac{\partial(\rho)}{\partial t} + \nabla.(\rho u) = 0 \quad (2)$$

$$\frac{\partial(\rho)}{\partial t} + \nabla.(\rho u.u) = -\nabla P + \nabla.[\mu(\nabla u + \nabla u^T)] + \rho g + F \quad (3)$$

In these equations, ρ represents the fluid density (kg/m³), t denotes time (s), u indicates the average velocity (m·s⁻¹), and P corresponds to pressure (N·m⁻²), g is gravitational acceleration (m. s^{-2}), and F corresponds to the external body force per unit volume (kg. m^{-2}. s^{-2}).

The VOF method enables the tracking of the fluid interface within the computational domain and calculates the volume fraction of each phase in every computational cell, as described in Eq. (4) and Eq. (5).

$$\rho = \rho_o \alpha_o + (1 - \alpha_0)\rho_w \quad (4)$$

$$\mu = \mu_o \alpha_o + (1 - \alpha_0)\mu_w \quad (5)$$

Where ρ_o denotes the density of oil (kg/m^3), α_o represents the volume fraction of oil, ρ_w is density of water (kg/m^3), μ_o denotes the viscousity of oil (kg/m.s), and μw denotes the viscousity of water (kg/m.s).

Surface tension is generated by the attractive forces between molecules at the interface of a fluid. Within the Continuum Surface Force (CSF) model, this effect is represented as a volumetric force, as expressed in Eq. (6), while the interface gradient formulation is presented in Eq. (7)–Eq. (9). The interaction between the fluid and the solid surface is accounted for by considering wall adhesion effects. This is described using θw, which denotes the equilibrium contact angle formed between the fluid and the wall, as expressed in Eq. (10).

$$F = \sigma\kappa \frac{\rho \nabla \alpha_o}{0.5(\rho_o + \rho_w)} \quad (6)$$

$$n = \alpha_o \quad (7)$$

$$\kappa = \nabla.\hat{n} \quad (8)$$

$$\hat{n} = \frac{n}{|n|} \quad (9)$$

$$\hat{n} = \hat{n}_w \cos\theta_w + \hat{t}_w \sin\theta_w \quad (10)$$

The governing equations outlined in this section represent the fundamental principles of mass and momentum conservation. As general formulations, they can be applied to pipe flow problems regardless of the specific geometry of the pipe.

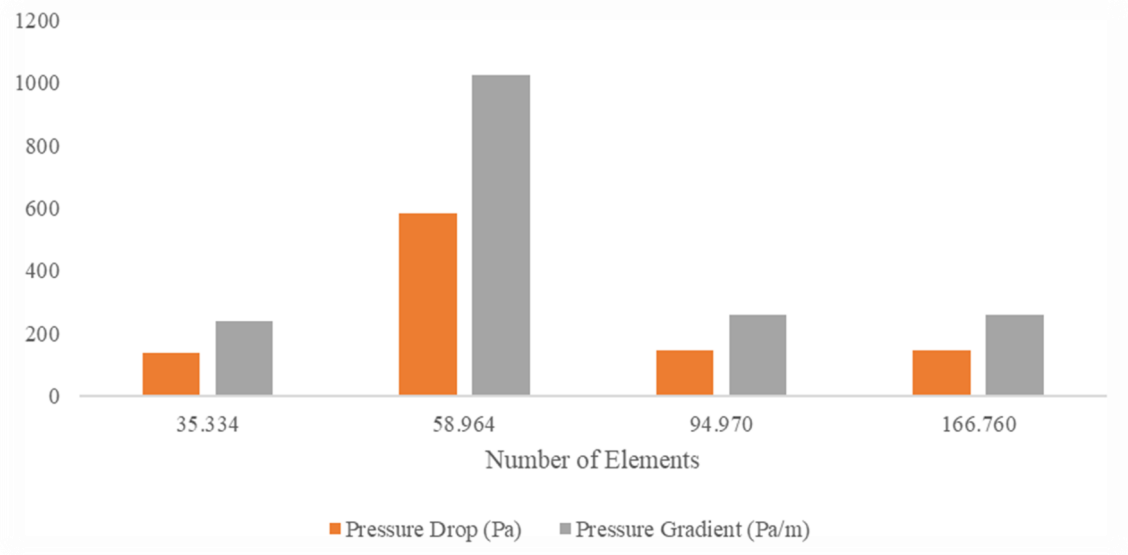

Figure 5. Pressure data of various numbers of elements comparison.

Boundary conditions

Boundary conditions are defined at the inlet for both the primary and secondary phases, as well as at the outlet and along the wall surfaces. Velocity magnitude input is performed at the inlet, adapted from Rodriguez and Bannwart (Rodriguez & Bannwart 2006). At the inlet, the oil enters the pipe as a central core, surrounded by a surrounding layer of water.

This section specifies the volumetric flow rates or superficial velocities (the volumetric flow rates of the phases per unit area) for both phases. The superficial velocities of the oil (Uo) and water (Uw) are given as 0.21 m/s and 0.058 m/s, respectively. Using the superficial velocity, the inlet velocity profile can be determined. The outlet is set to a constant pressure, and no-slip boundary conditions are applied at the wall.

RESULT AND DISCUSSION

Once the simulation is finished, CFD generates numerical results that describe how the fluid flows. These results can then be displayed visually using contour plots, vector fields, or streamline diagrams. Validation is performed by comparing these CFD results with experimental data to ensure accuracy and reliability. The following analysis examines the validated results in order to gain a more detailed understanding of the flow characteristics.

Comparison with experimental data

Interfacial wave geometry refers to the form and dynamic characteristics of the boundary that separates two phases in a multiphase flow. It involves features such as wave amplitude, wavelength, frequency, and the general shape of the interface as it evolves over time. In the reference experiment by Rodriguez and Bannwart (Rodriguez & Bannwart 2006), heavy crude oil (viscosity 500 mPa·s; density 930 kg/m³) was pumped after water, producing data on oil and water superficial velocities as well as interfacial wave characteristics, wavelength (ë), minimum radius (R_o), maximum radius (R_{max}), wave velocity (a), and oil holdup (ε), obtained through photographic and image-analysis techniques.

Using identical fluid properties, the current three-dimensional simulation determines the corresponding parameters after the transient analysis and pipe-length assessment verify that the flow has reached a fully developed state. The resulting water–volume-fraction contours indicate the formation of interfacial waves. Figure 6 presents a comparison between the experimentally observed wave pattern (Fig. 6a) and the corresponding simulation result (Fig. 6b).

In the visualization, red indicates regions with a high water fraction, while blue corresponds to the oil core. Both images display a bamboo-like wave structure. This pattern forms because the lighter oil phase moves faster than the surrounding water, which reduces the radius of the oil core and induces disturbances at the interface between the two fluids. Moreover, in upward vertical flow, the combined effects of buoyancy and pressure gradient stretch the core and enhances bamboo-like wave formation, whereas downward flow may compress the core and produce corkscrew patterns. Similar bamboo-like wave patterns have also been observed in other investigations of vertical conductive anodic filaments (CAF) (Bai, Chen, & Joseph, 1992).

From a quantitative perspective, the simulation corresponds closely with the experimental observations. The largest difference is 15.84% in wavelength, while the deviations for minimum radius, maximum radius, wave velocity, and oil holdup remain below 4%. The complete comparison of these values is summarized in Table 3.

From a physical perspective, changes in wavelength can be explained by the strong sensitivity of interfacial wave behavior in core–annular flow to even small variations in the inlet boundary conditions, surface wettability, and the presence of trace impurities, which inherently difficult to reproduce with exact fidelity in CFD simulations. In addition, the Volume of Fluid (VOF) method treats the interface as perfectly sharp and well-defined, while in real systems the boundary between oil and water can undergo slight mixing or micro-emulsification, particularly near wave crests, which can influence the experimentally measured wavelength.

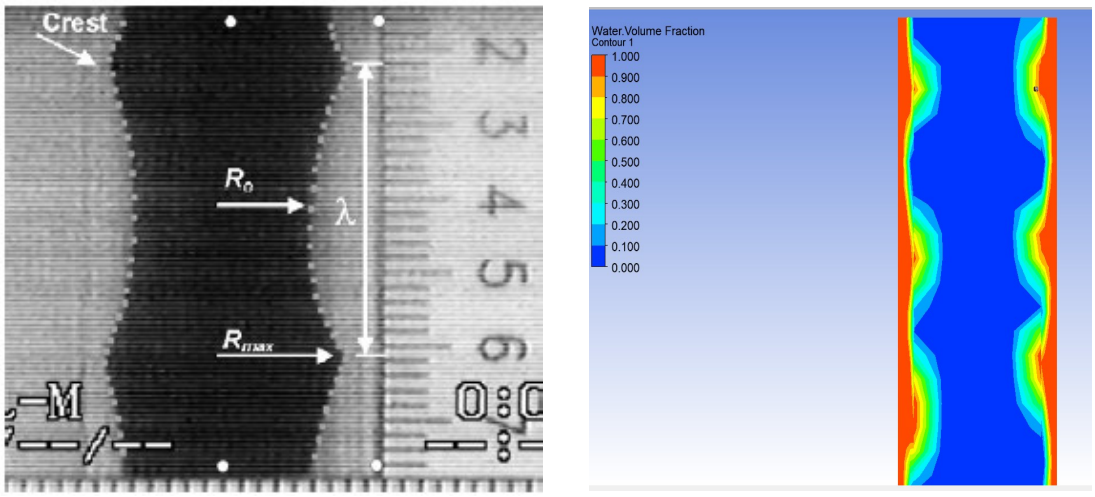

(a) (b)

Figure 6. Visual of interfacial wave of the top part of the pipe (a) experimental result (Rodriguez and Bannwart, 2006); (b) current simulation result.

From a numerical standpoint, the discrepancy observed can also be linked to the resolution of the mesh along the axial direction. Although grid independence has been verified, spatial discretization effects may still introduce a degree of numerical dissipation, leading to slight damping or elongation of the simulated interfacial wave structure. Despite this discrepancy, the extent of the deviation is still considered acceptable. Earlier studies on core–annular flow have documented wavelength variations of up to 17% while the overall hydrodynamic behavior remained consistent and reliable, thereby supporting the applicability and validity of the present simulation results (Babakhani Dehkordi, Azdarpour, & Mohammadian 2018).

Velocity profile

Figure 7 shows the progressive variation in velocity magnitude across the radial direction. This is obtained by extracting the velocity profile along the pipe and representing the data graphically. The pipe centre experiences the highest velocity, which progressively drops until it reaches zero at the wall. At the interface, corresponding to the observed position of the interface, the radial velocity gradient exhibits a sudden change at approximately 0.0113 m from the center of the pipe. The flow velocity along the pipe shows a value that can be said to be constant.

Fraction of volume

Figure 8 presents the oil volume fraction at several z/D locations. The highest concentration of oil is observed at the center of the pipe, whereas the level of fluctuation becomes more pronounced as it approaches the pipe wall. Ideally, oil holdup approaches 1 near the pipe centre (low r/R) and approaches 0 near the wall (high r/R), indicating that the oil core does not contact the wall. This observation aligns with the water–volume–fraction cross-section presented in Figure 9, which further verifies that no CAF fouling occurred. The fluctuating curves represent the formation of wavy core-annular flow (WCAF). WCAF represents the most common type of lubricated core flow and generally exhibits higher stability than perfect core-annular flow (PCAF) (Bai, Chen, & Joseph, 1992).

Pressure

Figure 10 presents the longitudinal variation of absolute pressure. This shows that as the flow moves toward the outlet, the pressure gradually drops. This phenomenon can be described using Bernoulli's equation. However, since the velocity is considered relatively constant, Bernoulli's equation (Eq. 11) can be simplified into Eq. 12.

Table 3. Interfacial wave geometry data.

Parameter	Run	Simulation	Experiment	Error
U_o (m/s)	1	0.21	0.21	
	2	0.35	0.35	
U_w (m/s)	1	0.06	0.06	
	2	0.06	0.06	
Wave Length (mm)	1	32.23	38.18	15.58%
	2	23.72	28.18	15.84%
R_o (mm)	1	10.33	10.13	1.97%
	2	11.61	11.37	2.15%
R_{max} (mm)	1	13.17	13.19	0.16%
	2	13.18	13.23	0.35%
a	1	0.28	0.27	2.91%
	2	0.36	0.37	3.57%
ε	1	0.62	0.63	2.21%
	2	0.70	0.72	2.42%

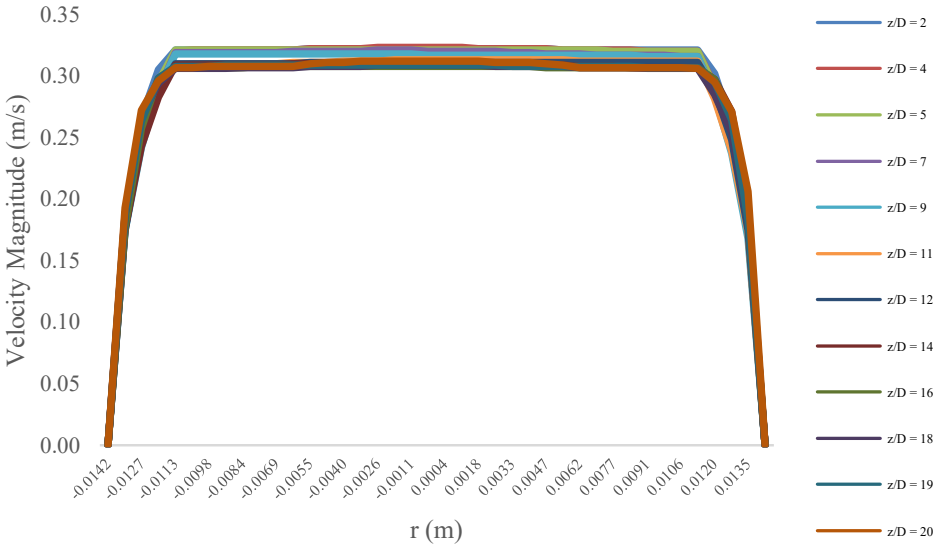

Figure 7. Velocity profile at different locations along pipe (z/D).

$$P_1+\rho g h_1 = P_2 + \rho g h_2 \quad (11)$$

where P is pressure, ρ is density, and h is height.

This relationship indicates that when the fluid velocity stays constant, an increase in pressure results in a decrease in height, and conversely, a decrease in pressure leads to an increase in height. The fluctuation is caused by the interface interaction between the two phases. Because the geometry does not contain any constriction or expansion, the resulting changes or fluctuations are minimal (Banerjee et al., 2024).

The pressure gradient can be determined by applying the pressure gradient equation developed for CAF under vertical upward flow conditions (Rodriguez & Bannwart, 2006). While the pressure gradient simulation results are obtained by processing the pressure drop data for total length from the pipe inlet to outlet.

$$G_f = \frac{\Delta P_{friction}}{H} = \frac{\Delta P_{dpt}}{H} - (\rho_1 - \rho_2) g \varepsilon \quad (12)$$

where ΔP_{dpt} is the pressure gradient, H is the length between the two pressure data collection areas, and ε is the in situ oil holdup.

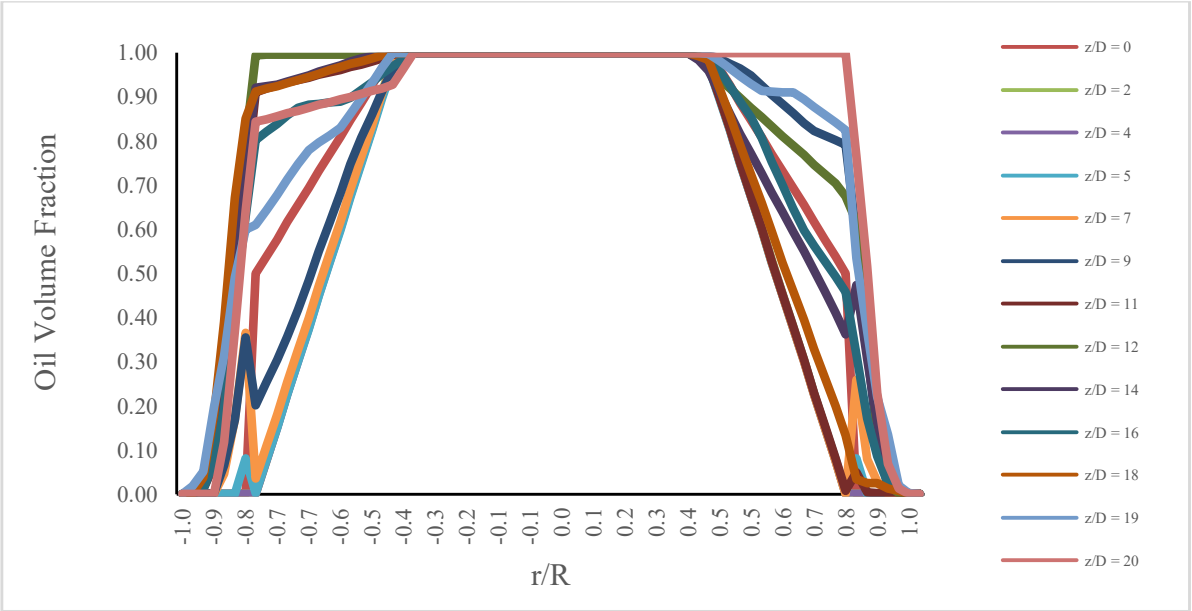

Figure 8. The volume fraction of oil that occurs at various heights (z/D) relative to the centre of the pipe (r/R).

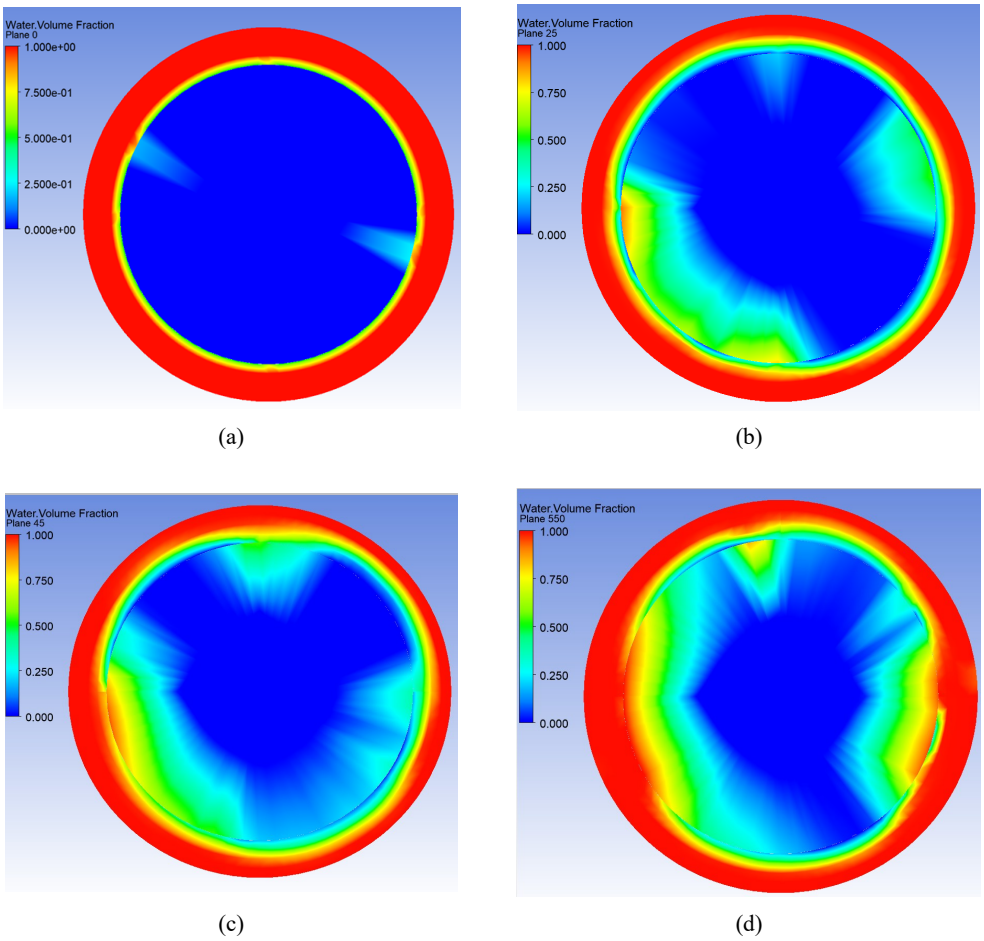

Figure 9. Cross-sectional contour of water volume fraction (a) z/D=0 (b) z/D=9 (c) z/D=16 (d) z/D=19.

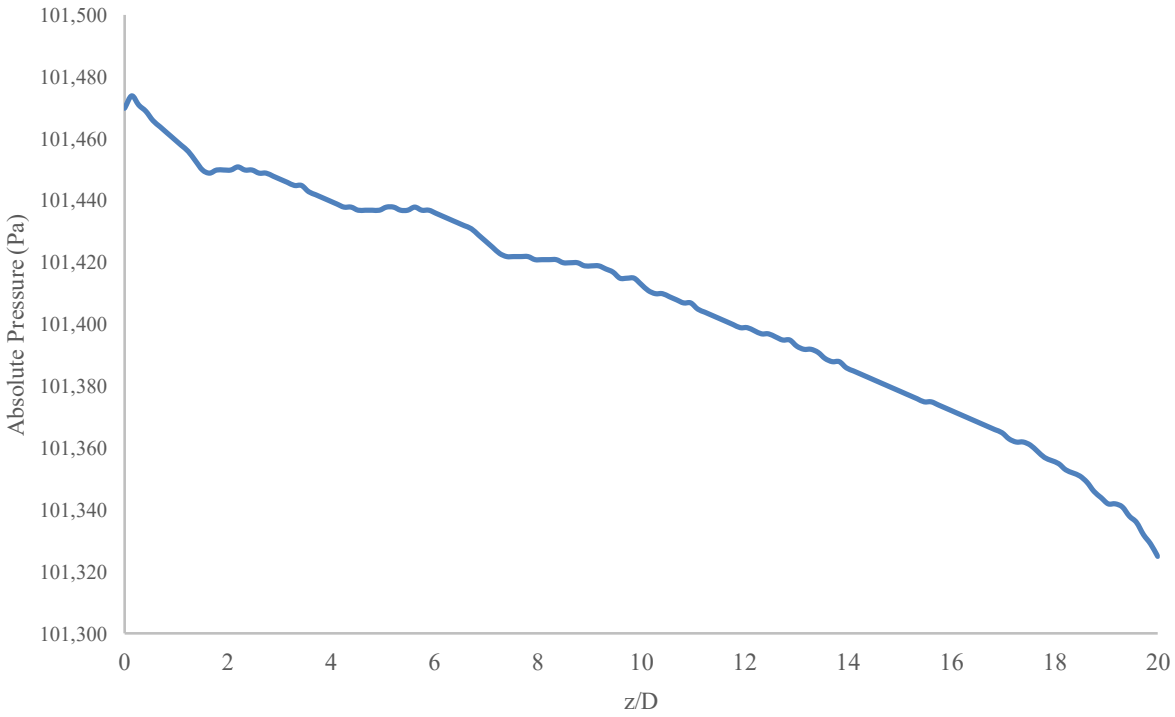

Figure 10. Absolute pressure profile of core annular flow.

The results of the calculations are presented in Table 4 and serve as a basis for validating the simulation, with differences from the theoretical predictions remaining within 20%. Furthermore, the pressure gradient from the three-dimensional simulation is compared with the two-dimensional results in Table 5.

The comparison indicates that the present simulation aligns closely with the theoretical formulation and yields a smaller percentage error than the two-dimensional simulation previously reported by Gupta in 2016 (Gupta et al., 2016).

Table 4. Pressure gradient result comparison.

Parameter	Simulation	Formula	Error
Pressure Gradient (Pa/m)	300.6819	314.4979	4.39%
Frictional Pressure Gradient (Pa/m)	258.3979	216.3364	19.44%

Table 5. Frictional pressure gradient result comparison of the simulations.

Calculation	Pressure gradient (Pa/m)	Error
3D CFD Simulation (current work)	258.3979	19.44%
2D CFD Simulation (Gupta, 2016)	26.40845	87.79%
Formula	216.3364	-

Effect of gravity

In core-annular flow (CAF), the oil core is buoyantly supported by the surrounding water layer. During upward vertical flow, the overall pressure drop results from the combined effects of gravitational forces and friction along the pipe wall. Without gravity, only friction opposes the flow, but with gravity, the fluid weight creates an additional opposing force while buoyancy acts in the flow direction. This trend is illustrated in Table

6, where a comparison of pressure drops and pressure gradients under conditions with and without gravity indicates that the zero-gravity case produces a lower pressure drop.

Table 6. Frictional pressure gradient result comparison of the simulations.

Case	Pressure drop (Pa)	Pressure gradient (Pa/m)
No Gravity	15.07	26.5317
With Gravity	146.77	258.3979

Figure 11 also shows that the pressure in the case without gravity is lower compared to the case where gravity is included, which is a maximum of 8.615 Pa when compared to the pressure working on the case with gravity in the same observation area, which is a maximum of 82.862 Pa.

Wall shear stress

Changes in wall shear stress significantly affect the distribution of frictional force and flow behavior along a pipe (Cadence 2022). In core annular flow (CAF), the differences in viscosity and velocity between the core fluid and the surrounding annular fluid lead to variations in wall shear stress. As illustrated in Figure 12, the shear stress initially decreases and then shows a slight increase.

To compare, a single-phase heavy-oil simulation was performed using identical geometry, fluid properties, and flow rate (0.1212 kg/s). The wall shear stress distribution presented in Figure 13 indicates significantly higher values, reaching up to 344.2 Pa. This occurs because the high viscosity of the oil produces greater friction along the pipe wall, which aligns with the principle that shear stress increases proportionally with viscosity.

The pressure profile of the single-phase flow in Figure 14 is also higher and smoother than in CAF. In the absence of a lubricating water layer, the flow experiences higher resistance, which results in a larger pressure drop. Consequently, the characteristic fluctuations observed in core annular flow (CAF) disappear, since they are normally caused by interactions at the oil–water interface.

Energy savings

The evaluation of potential energy savings is conducted using the formula introduced by Coelho (2020), which was specifically developed for the CAF case and is summarized in Table 7. Evaluating energy savings in pumping heavy oil using CAF is completed by comparing the total hydraulic power (Ψ) required to pump a certain amount of oil using single-phase oil flow with that required to pump heavy oil with the exact quantity of oil through an oil-water fluid flow.

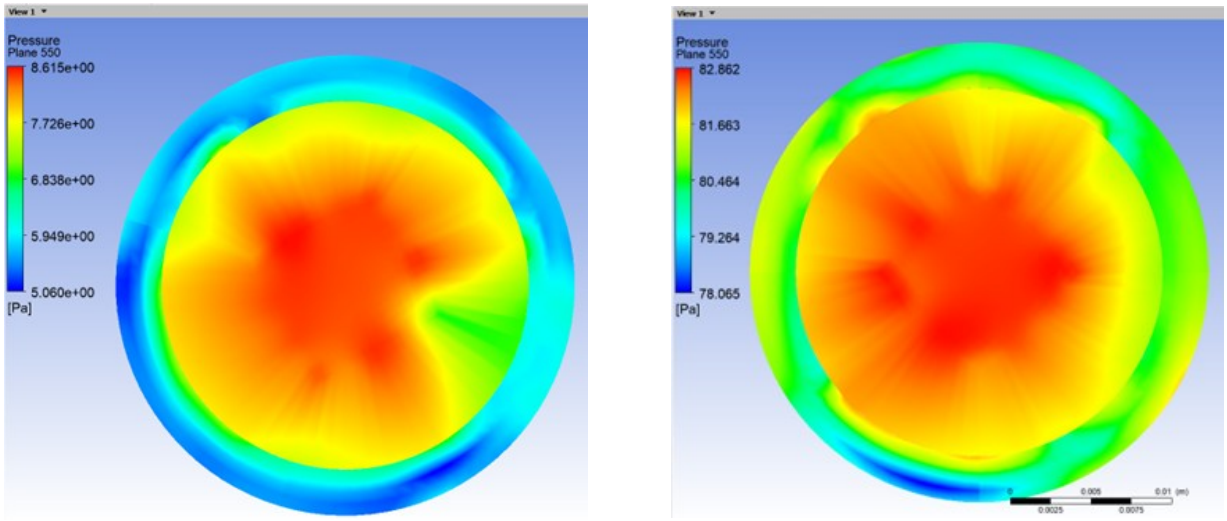

(a) (b)

Figure 11. Pressure at z=550 mm for (a) No Gravity Case (b) Case with Gravity.

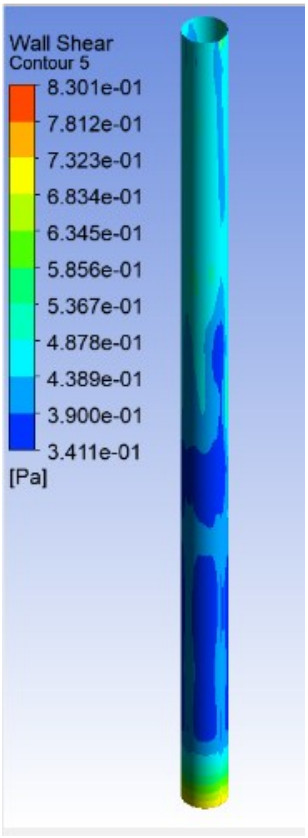

Figure 12. Wall shear contour of core annular flow.

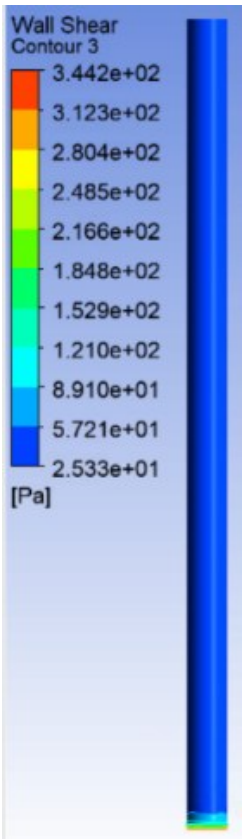

Figure 13. Wall shear contour of single-phase oil flow.

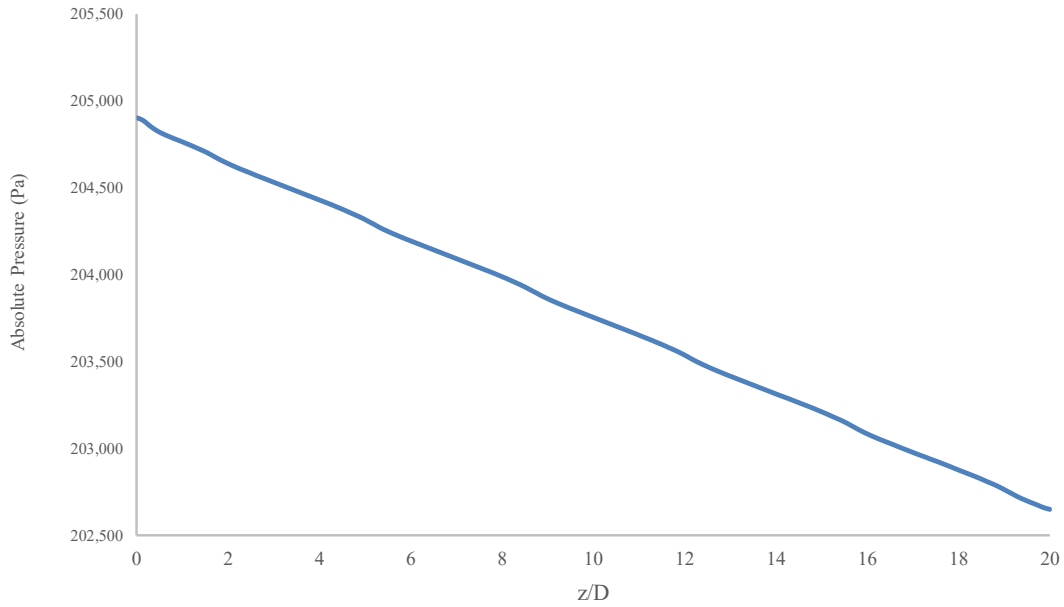

Figure 14. Wall Shear Contour of Single-Phase Oil Flow.

Table 7. Pump hydraulic power of systems.

Flow system	Volumetric flow rate (m3/s)	ΔP (Pa)	Ψ (Watt)
Single Phase Oil	1.3031×10^{-4}	2287.03	0.3022
Core Annular Flow	1.7921×10^{-4}		0.0264
Annulus (Water)	4.8901×10^{-5}	146.77	0.0072
Core (Heavy Oil)	1.3031×10^{-4}		0.0192

Following the calculation of the pump's hydraulic power, the absolute energy required by the pump to transport one unit volume of heavy oil was determined for both single-phase oil transport (ES) and two-phase oil–water transport (EB). The resulting energy consumptions were 2287.03 J/m³ and 201.85 J/m³, respectively.

In other words, the energy saving of CAF in this case is 91.17 % with a power reduction factor is 11.33 or about 93.58% pressure drop reduction. A larger reduction factor in power consumption indicates that the two-fluid flow process operates with greater energy efficiency. In addition, the power reduction factor greater than 1 indicates that the two-phase system is more energy-efficient than the single-phase oil system (Coelho et al., 2020).

Energy savings can also be assessed using another parameter. Peysson (Peysson et al., 2005) analyzed lubrication efficiency by measuring the percentage reduction in pressure drop, expressed as ÄP*. Current work shows ΔP* of 93.58% and a pressure reduction factor of 15.58 times. Another calculation of ΔP* in CAF has been done before, with values of 94% up to 98% (Dianita, Piemjaiswang, & Chalermsinsuwan 2023). The reduction in pressure drop observed in this study falls within the range previously reported in earlier research. This energy savings is strongly related to the low wall shear stress occurring along the pipe wall because of water lubrication. Moreover, the wavy CAF demonstrates higher energy efficiency compared with the perfect CAF configuration (Joseph et al., 1992).

CONCLUSION

This study carried out a three-dimensional CFD simulation of upward vertical core–annular flow using parameters derived from experimental conditions. The simulation was able to replicate the shape and behavior of the interfacial waves, showing good agreement with the patterns observed in the experiments. The bamboo-wave CAF pattern reflects the influence of buoyancy and

pressure gradients, which stretch the oil core in upward flow. The simulation results demonstrate a strong quantitative agreement with the experimental data. The largest deviation observed is 15.6% in the wavelength, while the differences for the minimum radius, maximum radius, wave velocity, and oil holdup remain below 3%. The pressure gradient is only 4.4% lower than the theoretical value, and compared with a previously reported 2D simulation, this 3D model provides more accurate flow patterns and hydrodynamic predictions.

The hydrodynamic analysis indicates the formation of a stable velocity profile throughout the flow. The oil phase maintains the highest volume fraction within the core region, while the absolute pressure gradually decreases along the pipe length. In addition, the wall shear stress distribution highlights the lubricating advantage provided by the CAF layer. Flow with gravity also produces a higher pressure drop. Ultimately, the energy assessment shows that the system can achieve energy savings exceeding 90%, suggesting strong potential for practical heavy-oil transport, although larger-scale studies are still required.

ACKNOWLEDGEMENT

This work is supported by the Ministry of Higher Education, Science, and Technology of the Republic of Indonesia through the 2025 Reputable Journal Publication Assistance Program.

GLOSSARY OF TERMS AND SYMBOLS

Terms & Symbols	Definition	Unit
Core-Annular Flow (CAF)	A flow regime where a high-viscosity fluid (heavy oil) forms a core in the center of the pipe, surrounded by a low-viscosity fluid (water) annulus, significantly reducing the frictional pressure drop during transport.	-
Non-Newtonian Fluid	A fluid whose viscosity is not constant and varies based on the applied shear rate; heavy crude oil often exhibits shear-thinning properties, unlike water, which is a Newtonian fluid.	-
Computational Fluid Dynamics (CFD)	A branch of fluid mechanics that utilizes numerical analysis and data structures to solve and analyze problems that involve fluid flows, such as simulating the interface fluctuation between oil and water phases.	-
Buoyancy Force	An upward force exerted by a fluid that opposes the weight of an immersed object; in vertical CAF pipelines, this force helps center the light oil core, providing greater stability compared to horizontal configurations.	N
Eccentricity	The measure of deviation of the oil core from the center of the pipe; in horizontal flows, density differences often cause high eccentricity, leading to potential oil fouling on the pipe walls.	-
Interfacial Tension (IFT)	The cohesive force acting at the boundary between two immiscible fluids (e.g., oil and water), which plays a critical role in maintaining the stability of the water annulus and preventing the breakup of the oil core.	N/m
Shear-Thinning	A characteristic of certain non-Newtonian fluids where viscosity decreases under shear strain; this property is significant when analyzing the flow behavior of heavy crude oil under high-velocity conditions.	-
Waxy Crude Oil	A type of petroleum containing paraffin wax that can crystallize at lower temperatures; its transport requires careful analysis of heat transfer to prevent solidification and blockage.	-
Pressure Gradient	The rate at which pressure changes along a given distance in the pipeline; the primary goal of introducing a water annulus in CAF is to lower this gradient compared to single-phase oil transport.	Pa/m
Volume of Fluid (VOF)	A specific numerical technique used in CFD to track the position and shape of the interface between two or more immiscible fluids (like oil and water) within a computational grid.	-

REFERENCES

ANSYS Inc., 2021. CFD Experts Simulate the Future.

ANSYS Inc., 2023a. Ansys Fluent Theory Guide.

ANSYS Inc., 2023b. ANSYS Fluent Tutorial Guide 18. ANSYS Fluent Tutorial Guide, 15317 (April), pp.724–746.

Babakhani Dehkordi, P., Azdarpour, A. & Mohammadian, E., 2018. Hydrodynamic behavior of high viscous oil–water flow through horizontal pipe undergoing sudden expansion—CFD study and experimental validation. Chemical Engineering Research and Design, 139, pp.144–161. doi:10.1016/j.cherd.2018.09.026.

Bai, R., Chen, K. & Joseph, D.D., 1992. Lubricated pipelining: Stability of core-annular flow. Part 5: Experiments and comparison with theory. Journal of Fluid Mechanics, 240, pp.97–132. doi:10.1017/S0022112092000041.

Banerjee, S., Banik, A., Rajak, V.K., Bandyopadhyay, T.K., Nayak, J., Jasinski, M., Kumar, R., Jeon, B.-H., Siddiqui, M.R., Khan, M.A., Chakrabortty, S. and Tripathy, S.K., 2024. Two-Phase Crude Oil–Water Flow Through Different Pipes: An Experimental Investigation Coupled with Computational Fluid Dynamics Approach, ACS Omega, 9(10), pp. 11181–11193. https://doi.org/10.1021/acsomega.3c05290.

Cadence, 2022. The relationship between wall shear stress and the maximum shear stress formula [WWW Document]. Cadence.

Çengel, Y. A. and Ghajar, A. J., 2025. Heat and Mass Transfer: Fundamentals and Applications. 7th edn. New York, NY: McGraw-Hill Education.

Coelho, N. M. D. A., Ribeiro, G. C. P., do Nascimento, M. M., de Souza, A., Soares, E. J., Bannwart, A. C., 2020. Energy savings on heavy oil transportation through core annular flow pattern: An experimental approach. International Journal of Multiphase Flow, 122, p.103127. doi:10.1016/j.ijmultiphaseflow.2019.103127.

Dianita, C., Piemjaiswang, R., Chalermsinsuwan, B., 2023. Computational fluid dynamics approach for energy savings evaluation in core annular flow of a horizontal T-pipe. Energy Reports 9, 8–15. https://doi.org/10.1016/j.egyr.2023.05.218

Dianita, C., Faturahman, M. & Mardianza, A., 2025. Pore-scale 3D modeling of viscous fingering for non-Newtonian heavy oil recovery. Scientific Contributions Oil and Gas, 48(1), pp.77–90. https://doi.org/10.29017/scog.v48i1.1690

Gupta, R., Turangan, C. & Manica, R., 2016. Oil-water core-annular flow in vertical pipes: A CFD study. Canadian Journal of Chemical Engineering, 94, n/a. doi:10.1002/cjce.22451.

Kim, J. and Park, H., 2024. Characteristics of turbulent core–annular flow with water-lubricated high viscosity oil in a horizontal pipe, Journal of Fluid Mechanics, 986, p. A15. doi:10.1017/jfm.2024.345

Lintermann, A., 2021. Computational Meshing for CFD Simulations. pp. 85–115. https://doi.org/10.1007/978-981-15-6716-2_6

Peysson, Y., Bensakhria, A., Antonini, G., Argillier, J. F. 2005. Pipeline lubrication of heavy oil: Experimental investigation of flow and restart problems. In: SPE International Thermal Operations and Heavy Oil Symposium.

Rodriguez, O.M.H. & Bannwart, A.C., 2006. Experimental study on interfacial waves in vertical core flow. Journal of Petroleum Science and Engineering. doi:10.1016/j.petrol.2006.07.007.

Silva, B. F., Magalhães, H. L. F., Gomez, R. S., Cabral, E. de M., Batista, F. A., Pereira, A. B. da C., Lima, W. M. P. B. de, Lima, A. G. B. de, 2020. Isothermal Transport (Core-Flow Type) of Heavy and Ultraviscous Oil in Curved Pipes: A Transient Study by CFD. Open Journal of Fluid Dynamics 10, 122–134. https://doi.org/10.4236/ojfd.2020.102008

Susantoro, T. M., Suliantara, Setiawan, H. L., Widarsono, B., Wikantika, K., 2022. Heavy Oil Potentials in Central Sumatra Basin, Indonesia Using Remote Sensing, Gravity, and Petrophysics Data: From Literature Review to Interpretations and Analyses. Indonesian Journal of Science and Technology 7, 363–384. https://doi.org/10.17509/IJOST.V7I3.51288

Widarsono, B. et al., 2021. An integrated approach for revisiting basin-scale heavy oil potential of the Central Sumatera Basin. Scientific Contributions Oil and Gas, 44(1), pp.1–20. https://doi.org/10.29017/SCOG.44.1.493

Xie, B., Jiang, F., Xiang, J. and Ye, C., 2023. Review of Core Annular Flow, Energies, 16(3), p. 1475. https://doi.org/10.3390/en16031496